Water Research 163 (2019) 114856

Contents lists available at ScienceDirect

Water Research

journal homepage: www.elsevier.com/locate/watres

Application of dynamic current density for increased concentration factors and reduced energy consumption for concentrating ammonium by electrodialysis

Niels van Linden*, Henri Spanjers, Jules B. van Lier

Delft University of Technology, Faculty of Civil Engineering and Geosciences, Stevinweg 1, 2628, CN Delft, the Netherlands

ARTICLE INFO

Article history:
Received 27 March 2019
Received in revised form
26 June 2019
Accepted 11 July 2019
Available online 12 July 2019

Keywords:
Electrodialysis
Ammonium
Current efficiency
Back-diffusion
Osmosis
Electro-osmosis

ABSTRACT

Ammonium (NH_4^+) can be recovered from water for fertiliser production or even energy production purposes. Because NH_4^+ recovery is more effective at increased concentrations, electrodialysis (ED) can be used to concentrate NH_4^+ from side streams, such as sludge reject water, and simultaneously achieve high NH_4^+ removal efficiencies. However, the effect of osmosis and back-diffusion increases when the NH_4^+ concentration gradient between the diluate and the concentrate stream increases, resulting in a limitation of the concentration factor and an increase in energy consumption for NH_4^+ removal. In this study, we showed that operation at dynamic current density (DCD) reduced the effect of osmosis and back-diffusion, due to a 75% decrease of the operational run time, compared to operation at a fixed current density (FCD). The concentration factor increased from 4.5 for an FCD to 6.7 for DCD, while the energy consumption of 90% NH_4^+ removal from synthetic sludge reject water at DCD remained stable at 5.4 MJ·kg-N^{-1}.

1. Introduction

1.1. Current side stream ammonia treatment

After organic protein degradation, ammonia (NH_3) ultimately ends up in wastewater streams in the form of ammonium (NH_4^+), which is an aqueous pollutant because the excessive discharge of NH_4^+ to receiving water bodies leads to eutrophication and subsequent oxygen depletion. Traditionally, NH_4^+ removal in wastewater treatment plants is achieved by the energy-intensive nitrification-denitrification process. By means of side stream treatment of the liquid fraction of sludge digestate (reject water) by the more energy-efficient anammox process, the total NH_4^+ load to the nitrification-denitrification can be reduced by 15–25%, resulting in a reduction of the total energy consumption of the wastewater treatment plant, compared to no reject water treatment (Van Hulle et al., 2010; Lackner et al., 2014). In the review of Magri et al. (2013), it is mentioned that the side stream removal of NH_4^+ requires 57 MJ·kg-N^{-1} by means of nitrification-denitrification via nitrite and that partial nitrification + anammox requires 19 MJ·kg-N^{-1}. Furthermore, Lackner et al. (2014) later reported that the energy consumption of side stream NH_4^+ removal in full-scale partial nitrification + anammox installations ranges only 3–15 MJ·kg-N^{-1}.

In the last two decades, there has been a growing interest for the recovery of NH_4^+ from residual (waste) waters as a resource for fertilisers, using mature technologies such as struvite precipitation and air stripping (Mehta et al., 2015). In addition, (bio-)electrochemical technologies such as microbial fuel cells, microbial electrolysis cells and electrochemical cells are widely studied for recovery of NH_4^+ from side streams such as reject water and urine, according to the review of Kuntke et al. (2018), who reported on more than thirty studies on electrochemical NH_4^+ recovery. However, the recovery of NH_4^+ from side streams still faces many challenges; low NH_4^+ transport fluxes and limited NH_4^+ removal efficiencies for bio-electrochemical systems and high energy and chemical consumption for the mature technologies and electrochemical cells (Mehta et al., 2015; Kuntke et al., 2018).

1.2. Ammonia as an energy source

Interestingly, NH_3 was recently identified as a suitable energy carrier, being an alternative to carbon-based energy carriers (ISPT,

* Corresponding author.Faculty of Civil Engineering, Department Watermanagement, the Netherlands.
E-mail address: N.vanLinden@tudelft.nl (N. van Linden).

https://doi.org/10.1016/j.watres.2019.114856

2017). The chemically bound energy in NH_3 (21 MJ·kg-N^{-1}, lower heating value at T = 700 °C) can be converted into electricity and heat by internal NH_3 cracking and subsequent hydrogen oxidation in a solid oxide fuel cell (SOFC), with nitrogen gas and water as final products (Wojcik et al., 2003). The SOFC is recognised as a very efficient technology to convert chemical energy to electrical energy, with an electrical efficiency of 60%, while an additional 30% of the converted chemical energy can be used as high-quality heat (Stambouli and Traversa, 2002).

1.3. Need to concentrate ammonium

The use of NH_3 as a fuel for SOFCs opens opportunities for energy production from NH_3 recovered from residual waters. However, to convert the chemically stored energy in NH_3, it must firstly be stripped from the water. NH_3 stripping is more effective at higher feed concentrations and when the medium pH is increased, commonly done by chemical addition or CO_2 stripping, converting NH_4^+ to NH_3 ($pK_a = 9.25$). After pH increase, NH_3 stripping can be achieved by vacuum membrane stripping (VMS), allowing for direct recovery of gaseous NH_3. Literature on (vacuum membrane) stripping of NH_3 shows that at higher concentrations of NH_3 in the liquid feed, higher mass fractions of NH_3 in the gaseous permeate can be obtained (El-Bourawi et al., 2007; He et al., 2018). In addition, literature reports that in SOFCs, higher mass fractions of NH_3 gaseous feed lead to higher power densities (Cinti et al., 2016). Therefore, to allow for better stripping of NH_3 for fertiliser production or energy production purposes, NH_4^+ in side streams should be concentrated.

1.4. Concentrating ammonium by electrodialysis

In this study, electrodialysis (ED) is used to concentrate NH_4^+, because it simultaneously concentrates NH_4^+ in the concentrate stream and achieves high NH_4^+ removal efficiencies in the diluate stream (the feed water). Pronk et al. (2006) removed NH_4^+ for 85% from source-separated urine for nutrient recovery purposes and concentrated NH_4^+ by a factor of 3.2 with an energy consumption of 96 MJ·kg-N^{-1}. In addition, Mondor et al. (2008) and Ippersiel et al. (2012) used ED for NH_4^+ recovery from digested swine manure and removed 75% and 87%, respectively, while achieving a concentration factor for NH_4^+ of 2.8 and 5.6, respectively. The energy consumption for removing and concentrating NH_4^+ in these two studies ranged 18–71 MJ·kg-N^{-1}. Furthermore, Wang et al. (2015) achieved full removal of NH_4^+ from sludge reject water by ED for nutrient recovery purposes and obtained a concentration factor of 18. However, the energy consumption was much higher than the other reported studies: 202–258 MJ·kg-N^{-1}. Finally, Ward et al. (2018) used ED to recover NH_4^+ from sludge reject water on pilot scale, achieving a concentration factor of 8.5 for NH_4^+. However, the removal of NH_4^+ from the sludge reject water was limited to 23%, while the energy consumption for NH_4^+ removal was competitive to anammox: 18 MJ·kg-N^{-1}.

1.5. Problems with concentrating ammonium with electrodialysis

The concentration factor for concentrating ions by ED is limited by water transport (Pronk et al., 2006; Mondor et al., 2008; Rottiers et al., 2014; Ward et al., 2018). The ion concentration gradient that establishes across the membranes between the diluate and concentrate causes osmosis (Strathmann, 2004a), resulting in dilution of the concentrate. In addition, the ion concentration gradient causes the concentrated ions to diffuse from the concentrate back to the diluate (back-diffusion) (Strathmann, 2004b). The diffused ions need to be transported back and forth, requiring an additional supply of electrical charge (and thus consumed energy). Back-diffusion, therefore, results in a decrease in current efficiency (Strathmann, 2004b) and an increase in energy consumption. The reported studies on concentrating NH_4^+ by ED either applied a fixed voltage or a fixed current density (FCD). When a fixed voltage is applied, the limiting current density (LCD) may be exceeded at low ion concentrations in the diluate. Water dissociates into H^+ and OH^- when the LCD is exceeded, resulting in a decreased current efficiency and an increase in energy consumption (Strathmann, 2010). When an FCD is applied, a current density equal to or lower than the LCD of the aimed diluate ion concentration is applied. However, the application of low current densities leads to low ion transport fluxes, indicating inefficient use of membranes and high operational run times. By decreasing the operational run time, the effect of osmosis and back-diffusion can be decreased, because an ion concentration gradient will inevitably establish when concentrating ions such as NH_4^+.

1.6. Objective

Previous research has shown that ED can effectively be applied to remove NH_4^+ from side streams. In this study, we propose to operate ED at dynamic current density (DCD), to more efficiently use ion exchange membranes (reduce the required membrane area), to increase the concentration factor and reduce the energy consumption. For DCD operation, the current density is dynamically adjusted in agreement with the decreasing ion concentration of the diluate, without exceeding the LCD. The effect of the current density on the concentration factor and energy consumption was studied by assessing the water transport and the NH_4^+ current efficiency during sequencing batch experiments at both the application of an FCD and DCD.

2. Materials and methods

2.1. Materials

Fig. 1 presents a schematic representation of the used experimental set-up. We used a bench-scale PC-Cell 64002 ED cell, consisting of a Pt/Ir coated titanium anode and a V4A steel cathode, with an electrode area of 8 × 8 cm^2. In between the electrodes, a ten cell pair membrane stack was placed, consisting of two PCA SC cation exchange end (CEEM), ten PCA SA standard anion exchange (AEM) and nine PCA SK standard cation exchange membranes

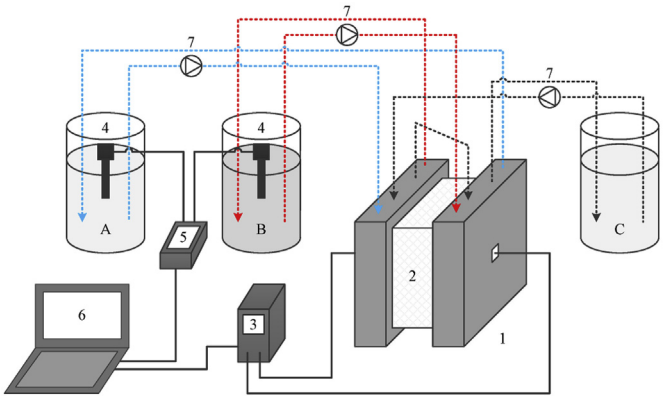

Fig. 1. A schematic representation of the used experimental set-up, including the ED cell (1), membrane stack (2), power supply (3), EC sensors (4), multimeter (5), laptop (6), peristaltic pumps (7) and the diluate (A), concentrate (B) and electrode rinse (C) solution.

(CEM) (PCA, 2016). The membrane stack contained polyethylene/silicone spacers to separate the electrodes and membranes, creating electrode rinse, diluate and concentrate channels. The spacers had a thickness of 0.5 mm and a void fraction of 59%. The lay-out of the electrodes, flow channels and membranes is schematically represented in Fig. 2.

The diluate and concentrate solutions were recirculated through the ED cell at a cross-flow velocity of 2 cm s^{-1}, following the recommendations of Strathmann (2010). The cross-flow velocity was controlled by using a calibrated peristaltic Watson-Marlow 520S pump at a flow rate of 19 L h^{-1}. The electrodes were rinsed with an electrode rinse solution at the same flow rate used for the diluate and concentrate. Separate Watson-Marlow 323 pump heads were used for each solution. For the application of electrical current, a Tenma 72–2535 power supply with an electrical current and electrical potential range of 0.001–3.000 A and 0.01–30.00 V, respectively, was used. The electrical conductivity (EC) and pH of the electrode rinse, diluate and concentrate were measured in the respective solution bottles, using two calibrated TetraCon 925 EC-sensors and a calibrated IDS SenTix 940 pH sensors, respectively, on a WTW Multi 3630 IDS multi-meter. NH_4^+ concentrations were measured with Machery-Nagel NANOCOLOR Ammonium 200 (range: 0.04–0.2 g L^{-1}) and 2000 (range: 0.4–2.0 g L^{-1}) test kits. Solution volumes were determined using calibrated volumetric cylinders.

Initial diluate and concentrate solutions consisting of 6.6 g L^{-1} NH_4HCO_3 were used, equal to an NH_4^+ concentration of 1.5 g L^{-1}, simulating NH_4^+ concentrations commonly present in sludge reject waters. We used synthetic solutions to be able to study the effect of back-diffusion and (electro-)osmosis as function of the NH_4^+ concentration gradient on the concentration factor and energy consumption at different current density operations. The initial electrode rinse solutions consisted of 1 M $NaNO_3$. The salts were of analytical grade (Sigma Aldrich Reagent Plus, ≥ 99%) and were added to 1 L of demi-water. The experiments were conducted at room temperature (T = 22 ± 1 °C).

2.2. Performance indicators

To assess water transport, we determined how much water was transported from the diluate to the concentrate. By relating the water transport to the initial water mass, the relative water transport was determined (Eq. (1)). Water transport to the electrode rinse was neglected, since only one diluate and concentrate channel were in contact with the electrode chambers. Besides, extra thick CEEMs were placed next to electrode compartments to minimise water transport.

$$\theta_{H_2O,t} = \frac{V_{i,d} \cdot \rho_{H_2O} - V_{f,d} \cdot \rho_{H_2O}}{V_{i,d} \cdot \rho_{H_2O}} \cdot 100\% \quad (1)$$

where $\theta_{H2O,t}$ = total water transport from the diluate (unitless), $V_{i,d}$ and $V_{f,d}$ = initial and final diluate volume, respectively (in L) and ρ_{H2O} = density of water (in g·L^{-1}, ρ_{H2O} = 995 g L^{-1} at T = 22 °C).

Water transport in ED is caused by an ion concentration gradient (osmosis), resulting in water transport from the diluate to the concentrate. In addition, water transport is caused by the application of electrical current, which causes water transport in the

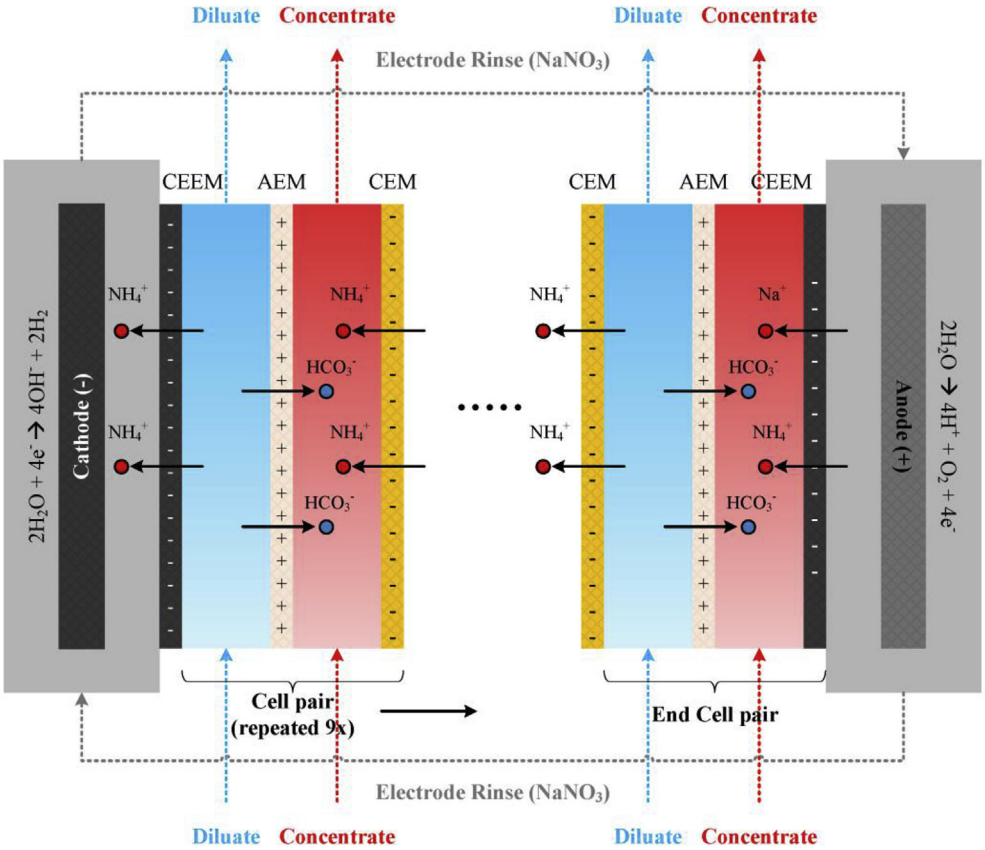

Fig. 2. A schematic representation of the membrane and flow channel sequence in the membrane stack, including ion transport due to the electrical current. The transport of cations at the electrodes through the CEEMs explains the accumulation of NH_4^+ in the electrode rinse: NH_4^+ is transported from the diluate to the electrode rinse at the cathode, while the same amount of charge transported through the CEEM at the anode is represented by both NH_4^+ and Na^+.

hydration shell of the transported ions from the diluate to the concentrate (electro-osmosis). The electro-osmotic water transport (Eq. (2)) was determined based on the amount of transported ions and their respective water transport numbers (Strathmann, 2004a). We assumed that for every transported mole of NH_4^+, 1 mol of HCO_3^- was transported to maintain charge balance in the diluate and concentrate flow channels. Based on the hydration numbers (amount of moles of water in the first hydration shell per mole of ions) determined in the studies of Brugé et al. (1999) and Leung et al. (2007), water transport numbers of four and seven were used for NH_4^+ and HCO_3^-, respectively, agreeing with the range of four to eight of Strathmann (2004a). The osmotic water transport was determined based on the mass balance of water transport (Eq. (3)).

$$\theta_{H_2O,e-o} = \frac{n_{NH_4^+,d} \cdot (T_w^{NH_4^+} + T_w^{HCO_3^-}) \cdot MW_{H_2O}}{V_{i,d} \cdot \rho_{H_2O}} \cdot 100\% \quad 2$$

where $\theta_{H2O,e\text{-}o}$ = electro-osmotic water transport (unitless), $n_{NH4+,d}$ = amount of transported diluate NH_4^+ (mol), T_w^{NH4+} and $T_w^{HCO3-} = NH_4^+$ and HCO_3^- water transport number, respectively (unitless) and MW_{H2O} = molecular weight of water (in $g \cdot mol^{-1}$, $MW_{H2O} = 18\ g\ mol^{-1}$).

$$\theta_{H_2O,o} = \theta_{H_2O,t} - \theta_{H_2O,e-o} \quad 3$$

where $\theta_{H2O,o}$ = osmotic water transport (unitless).

We determined the NH_4^+ current efficiency (Eq. (4)) by the transported charge as NH_4^+, relative to the total supplied electrical charge. Finally, the energy consumption to remove and concentrate NH_4^+ (Eq. (5)) was determined based on the mass of transported NH_4^+ from the diluate and the total used electrical energy to transport NH_4^+.

$$\eta_{NH_4^+} = \frac{z \cdot F \cdot n_{NH_4^+,d}}{N \cdot \sum_{t=0}^{t} (I_t \cdot \Delta t)} \cdot 100\% \quad 4$$

where $\eta_{NH4+} = NH_4^+$ current efficiency (unitless), z = ion valence (unitless, z = 1 for NH_4^+), F = Faraday constant (in $C \cdot mol^{-1}$, $F = 96{,}485\ C\ mol^{-1}$), N = number of cell pairs (unitless), I_t = electrical current (in A) and Δt = time interval (in s).

$$E = \frac{\sum_{t=0}^{t} (U_t \cdot I_t \cdot \Delta t)}{m_{NH_4^+,d}} \quad 5$$

where E = energy consumption (in $MJ \cdot kg\text{-}N^{-1}$), U_t = electrical potential (in V) and $m_{NH4+,d}$ = amount of transported NH_4^+ from the diluate (in kg-N).

2.3. Methods

To determine the current densities for the application of an FCD and DCD, we experimentally determined the relationship between the diluate EC and the LCD. To this end, various dilutions of the initial diluate (1, 0.9, 0.8, 0.75, 0.6, 0.5, 0.25, 0.05 and 0.01) were prepared. Subsequently, the current density was increased with steps of $1.5\ A\ m^{-2}$, while the electrical current and electrical potential were logged automatically, to determine the LCD for each dilution following the method of Cowan and Brown (1959).

To avoid water dissociation in local ion depleted zones, Strathmann (2004d) recommends using a safety factor (SF < 1) for the application of LCD. Operating at DCD is thus similar to the application of LCD in batch mode while using a safety factor. We determined a safety factor for the LCD to apply DCD, representing an optimum between the operational run time and the energy consumption. To find an optimum for these quantities with different units, we normalised the operational run time (Eq. (6)) and energy consumption (Eq. (7)) for SF = 1. We assigned equal weights to operational and energy consumption, while in practice different weights can be assigned, to determine an economical (cost-based) optimum safety factor (Strathmann, 2004d). Safety factors of 0.5, 0.75 and 1 were used to experimentally determine the safety factor that represents an optimum between the operational run time and energy consumption.

According to theory, the operational run time to transport a fixed amount of charge as ions is minimal for SF = 1 and increases reciprocally for lower safety factors (see S.I.). The normalised operational run time as a function of the safety factor is therefore described by $\alpha = SF^{-1} - 1$. Contrarily, the energy consumption to transport a certain amount of charge as ions has a maximum at SF = 1 and decreases linearly for lower safety factors (see S.I.). Therefore, the normalised energy consumption as a function of the safety factor can be described by $\beta = SF$.

$$\alpha = \frac{t_{SF} - t_{SF=1}}{t_{SF=1}} \quad 6$$

$$\beta = \frac{E_{SF}}{E_{SF=1}} \quad 7$$

where α = normalised operational run time (unitless) and β = normalised energy consumption (unitless).

To dynamically set the electrical current, we developed a Python script that calculated the electrical current based on the real-time diluate EC, the used safety factor and the determined relationship between the diluate EC and the LCD. The diluate EC measurements were logged on a laptop every 5 s and subsequently, the laptop controlled the power supply automatically to apply the electrical current. Electrical current and electrical potential data logged every 5 s on the laptop. The data of the concentrate EC was stored on a multimeter and the pH of all solutions was manually measured before and after each run. For the three chosen safety factors, duplicate runs with fresh solutions were conducted, in which the diluate EC was always decreased to $1\ mS\ cm^{-1}$.

Finally, we conducted sequencing batch experiments (SBEs) in duplicate, to assess the water transport and NH_4^+ current efficiency and study the effect of the current density (an FCD and DCD) on the concentration factor and the energy consumption. For the first batch, fresh diluate, concentrate and electrode rinse solutions were used and the NH_4^+ concentrations and volumes of all solutions were measured. After that, the diluate EC was again decreased to $1\ mS\ cm^{-1}$ and the NH_4^+ concentration and volume of all solutions were measured to make water and NH_4^+ balances. For the subsequent nine batches, the diluate was replaced for a fresh diluate solution, and the concentrate and electrode rinse solutions of the previous batch were reused. The electrical current during the DCD SBE was again applied using the automated control based on the Python script.

3. Results

3.1. Determination of current densities

We found a linear ($R^2 = 0.92$) relationship between the diluate EC and the LCD at a cross-flow velocity of $2\ cm\ s^{-1}$ (Fig. 3A), which was used to determine the current densities for the application of an FCD and DCD in the SBEs. Subsequently, we determined an

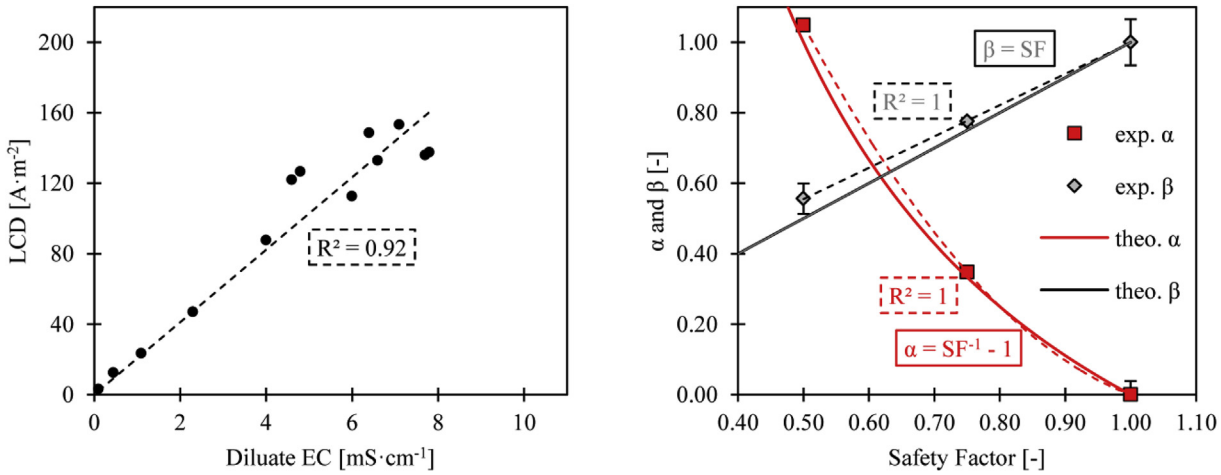

Fig. 3. The linear relationship between the diluate EC and the LCD (Fig. 3A). The theoretical (solid lines) and experimental (data points with error bars, representing the AVG ± STD for duplicate experiments, dashed lines representing the trend lines) α and β as a function of the safety factor for the LCD (Fig. 3B). An optimum was found at a safety factor of 0.62, representing an optimum between the operational run time and energy consumption.

optimum between the operational run time and the energy consumption by using a safety factor of 0.5, 0.75 and 1 for the LCD. Fig. 3B depicts the experimentally determined α and β as a function of the safety factor. The experimentally determined α had a minimum at SF = 1 and increased for lower safety factors. On the contrary, the experimentally determined β had a maximum at SF = 1 and decreased for lower safety factors. By means of fitting trend lines for the experimentally determined α and β, an optimum for the safety factor at 0.62 was found.

3.2. Sequencing batch experiment at a fixed current density

For the FCD SBE, a current density of 16 A m^{-2} was applied, based on the LCD of the final diluate EC (1 mS cm^{-1}) and a safety factor of 0.62. Fig. 4A presents the diluate and concentrate EC over the cumulative amount of consumed energy during the FCD SBE. The operational run time to decrease the diluate EC to 1 mS cm^{-1} increased by 58% over the number of batches, from 158 min for the first batch to 250 min for the tenth batch. Because the concentrate was recirculated during the SBE, the concentrate EC increased, but reached a plateau at 32 mS cm^{-1}.

From the NH_4^+ concentrations during the FCD SBE experiment (Fig. 4B), it follows that 91 ± 1% (AVG ± STD) of the NH_4^+ from the diluate was removed for all batches. The NH_4^+ concentration in the concentrate reached a plateau at 6.8 g L^{-1}, corresponding to a concentration factor of 4.5. The difference in concentration factor between the duplicate FCD SBEs was <5%. The increase in NH_4^+ concentration of the concentrate resulted in an increase in the NH_4^+ concentration gradient between the diluate and concentrate over the number of batches. The NH_4^+ concentration gradient was 2.4 g L^{-1} for the first batch, and increased to 6.6 g L^{-1} for the tenth batch. In addition to the diluate and concentrate NH_4^+ concentrations, Fig. 4B also presents the NH_4^+ concentration in the electrode rinse, showing that 21 ± 3% of the NH_4^+ transported from each diluate batch was transported to and accumulated in the electrode rinse.

The energy consumption increased over the number of batches, from 3.6 MJ·kg-N^{-1} for the first batch to 6.1 MJ·kg-N^{-1} for the tenth batch.

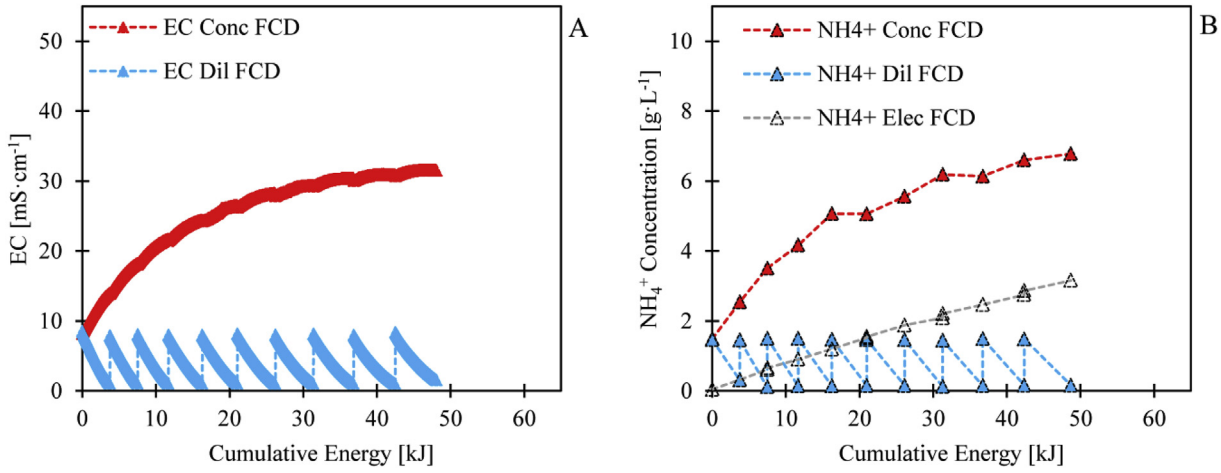

Fig. 4. The evolution of the EC (Fig. 4A) and NH_4^+ concentration (Fig. 4B) over the cumulative spent energy during the FCD SBE. The diluate EC was decreased to 1 mS cm^{-1} for every sequencing batch, corresponding to 91% (on average) removal of NH_4^+ from the diluate. The concentrate reached a plateau at 32 mS cm^{-1}, corresponding to an NH_4^+ concentration of 6.6 g L^{-1} and a concentration factor of 4.5. Besides transport of NH_4^+ from the diluate to the concentrate, 21% (on average) of the NH_4^+ was transported to and accumulated in the electrode rinse.

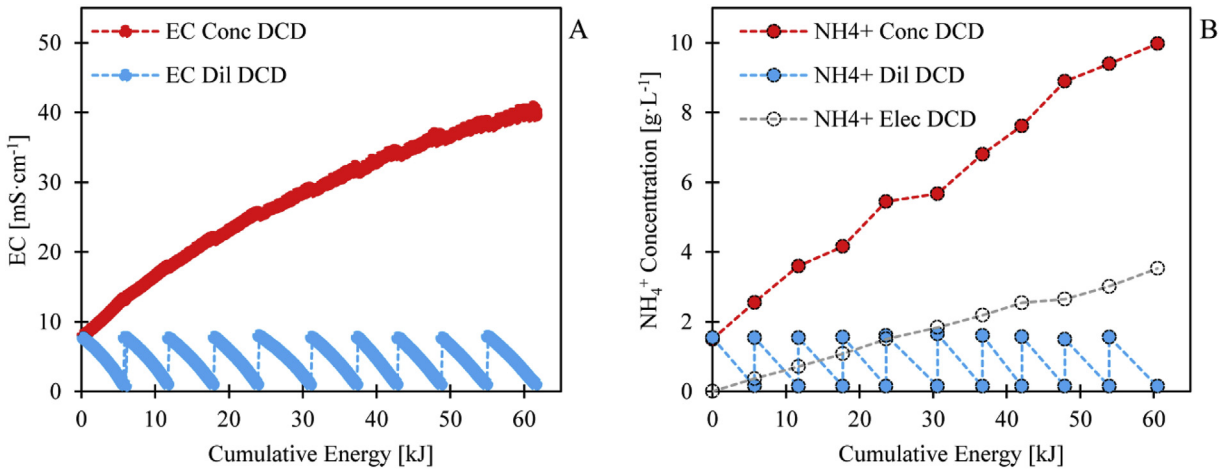

Fig. 5. The evolution of the EC (Fig. 5A) and NH_4^+ concentration (Fig. 5B) over the cumulative spent energy during the DCD SBE. The diluate EC was again decreased to 1 mS cm^{-1} for every sequencing batch, corresponding to 90% (on average) removal of NH_4^+ from the diluate. The EC and NH_4^+ concentration in the concentrate did not reach a plateau, but increased to 40 mS cm^{-1} and 10 g L^{-1} (concentration factor = 6.7), respectively. For the DCD SBE, 24% (on average) of the NH_4^+ accumulated in the electrode rinse.

3.3. Continuous batch experiment at dynamic current density

For the DCD SBE, a safety factor of 0.62 was used in combination with a variable current density, based on the LCD of the decreasing diluate EC. Fig. 5A presents the diluate and concentrate EC over the cumulative amount of consumed energy during the DCD SBE. Similar to the FCD SBE, the operational run time increased over the number of batches. However, the operational run time increased only by 29%, from 49 min for the first batch to 63 min for the tenth batch. The application of DCD resulted in a reduction of 69–75% of the operational run time, with respect to the application of an FCD. The reduced operational run time can be translated to a decreased in required membrane area to treat a certain volume of feed water. In addition, the concentrate EC did not reach a plateau and reached 40 mS cm^{-1} after ten batches.

During the DCD SBE, 90 ± 1% of the NH_4^+ from the diluate was removed for each sequencing batch, as follows from Fig. 5B. However, in contrast to the FCD SBE, the concentration of NH_4^+ in the concentrate did not reach a plateau, but increased linearly to 10 g L^{-1} after ten batches, corresponding to a concentration factor of 6.7. The difference in concentration factor between the replicate DCD SBEs was negligible: < 1%. The NH_4^+ concentration gradient increased from 2.4 g L^{-1} for the first batch to 9.8 g L^{-1} for the final batch. Similar to the FCD SBE, 24 ± 7% of NH_4^+ transported from the diluate accumulated in the electrode rinse during the DCD SBE.

In contrast to the increasing energy consumption during the FCD SBE, the energy consumption during the DCD SBE remained stable at 5.4 ± 0.4 MJ·kg-N^{-1}. The energy consumption of the tenth batch was lower for the application of DCD (5.9 MJ·kg-N^{-1}) than for the application of an FCD (6.1 MJ·kg-N^{-1}), while the NH_4^+ concentration gradient was actually higher for the application of DCD (9.8 g L^{-1}) than for an FCD (6.6 g L^{-1}).

4. Discussion

4.1. Determination of current densities

The found linear relationship between the diluate EC and the LCD corresponds with Strathmann (2004c), who reported that the LCD is linearly related to the diluate ion concentration for a specific flow channel geometry and cross-flow velocity.

In addition, an optimum between the operational run time and the energy consumption was experimentally found at a safety factor of 0.62. Fig. 3B also presents the theoretical α and β. Similar to the experimentally determined α and β, a theoretical optimum was found at a safety factor of 0.62, by equating the theoretical expressions for α and β.

4.2. Sequencing batch experiment at a fixed current density

The plateau of the NH_4^+ concentration in the concentrate, and thus the limitation of the concentration factor, was caused by water transport from the diluate to the concentrate. Fig. 6A shows how much water was transported during each batch by electro-osmosis and osmosis, as a function of the NH_4^+ concentration gradient. For the FCD SBE, osmosis was the dominant mechanism of water transport. The electro-osmotic water transport remained constant at 1.5% of the diluate throughout the SBE, because always the same amount of NH_4^+ was removed from the diluate (1.34 ± 0.02 g). The removal of NH_4^+ was constant because the diluate EC of the fresh solutions was always decreased to 1 mS cm^{-1}. The osmotic water transport increased from 2.5% at an NH_4^+ concentration gradient of 2.4 g L^{-1} to 10.5% at an NH_4^+ concentration gradient of 6.6 g L^{-1}. The increase in osmotic water transport was caused by two factors: because the NH_4^+ concentration gradient increased, the driving force for osmosis was higher and because the operational run time increased, more time was available to allow osmosis to take place.

NH_4^+ accumulation in the electrode rinse was caused by transport of NH_4^+ from the diluate through a cation exchange (end) membrane, ending up in the electrode rinse at the cathode side of the membrane stack. At the anode side of the membrane stack, an equivalent amount of charge migrated as cations from the electrode rinse to the concentrate. However, because the electrode rinse consisted of 1 M $NaNO_3$, the transported charge not only consisted of NH_4^+, but also of Na^+. This phenomenon is schematically presented in Fig. 2. By taking into account the accumulated NH_4^+ in the electrode rinse solution, the NH_4^+ mass balances fitted within 5%, while previous researchers assigned a 17–28% NH_4^+ loss to volatilisation of NH_3 from the diluate, concentrate and electrode rinse (Mondor et al., 2008; Ward et al., 2018).

Fig. 7A presents the NH_4^+ current efficiency over the NH_4^+ concentration gradient during the FCD SBE. The NH_4^+ current efficiency was 76% at an NH_4^+ concentration gradient of 2.4 g L^{-1} and decreased to 48% at an NH_4^+ concentration gradient of 6.6 g L^{-1}. In general, current efficiency in ED is mainly affected by water dissociation at current densities higher than the LCD, the transport

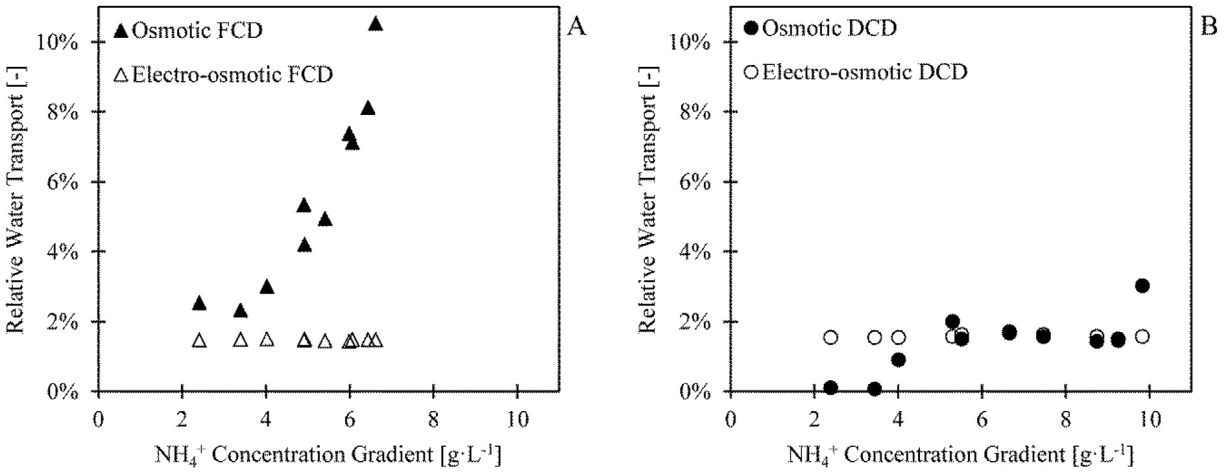

Fig. 6. The water transport during the FCD SBE (Fig. 6A) and the DCD SBE (Fig. 6B). During both SBEs, the electro-osmotic water transport was stable at 1.5–1.6% and the osmotic water transport for both SBEs increased over the NH_4^+ concentration gradient because both the driving force for osmosis and the operational run time increased.

of other ions than the target ion and back-diffusion (Strathmann, 2004b; Pronk et al., 2006). Because during the FCD SBE, the LCD was never exceeded due to the application of the safety factor, the effect of water dissociation on the NH_4^+ current efficiency was negligible. Besides, the pH ranged 7.8–8.8 throughout the entire SBE. At pH = 7.8, H^+ represented only $1.5 \cdot 10^{-3}$ C (as charge), while NH_4^+ in the initial diluate represented approximately 7500 C. In addition, Na^+ is transported from the electrode rinse solution to the concentrate and is therefore assumed not to be relevant for the assessment of the NH_4^+ current efficiency. Therefore, also the effect of the transport of other cations such as H^+ and Na^+ on the NH_4^+ current efficiency was negligible. According to Rottiers et al. (2014), the ion concentration gradient and back-diffusion are linearly related. Because during the FCD SBE the NH_4^+ current efficiency decreased over the increasing NH_4^+ concentration gradient, the decrease in the NH_4^+ current efficiency is assigned to back-diffusion, also in line with Pronk et al. (2006). During the FCD SBE, the NH_4^+ concentration gradient increased, resulting in a higher driving force for back-diffusion for each sequencing batch. Because back-diffusion took place from the concentrate to the diluate, NH_4^+ needed to be transported back and forth to decrease the diluate EC to 1 mS cm^{-1}, resulting in an increase in the operational run time. The transport of back-diffused NH_4^+ was at the expense of more supplied electrical charge, which led to a decrease in the NH_4^+ current efficiency. Because for each batch more back-diffusion took place over the number of batches, more electrical energy was required to transport NH_4^+ to decrease the diluate EC to 1 mS cm^{-1}. The energy consumption increased from 3.6 MJ·kg-N^{-1} to 6.1 MJ·kg-N^{-1} when the NH_4^+ concentration gradient increased from 2.4 g L^{-1} to 6.6 g L^{-1}, as presented in Fig. 7B.

4.3. Continuous batch experiment at dynamic current density

Fig. 6B depicts the water transport during the DCD SBE. For the first batches, electro-osmosis was dominant and only for later batches osmosis became the dominant water transport mechanism. The electro-osmotic water transport of 1.6% was constant during the DCD SBE and was similar to the electro-osmotic water transport during the FCD SBE (1.5%). The osmotic water transport was only 0.1% at an NH_4^+ concentration gradient of 2.4 g L^{-1} and increased to 3% at an NH_4^+ concentration gradient of 9.8 g L^{-1}. Since the osmotic driving force was higher during the DCD SBE than the during FCD SBE, the decrease in osmotic water transport is caused by the decreased operational run time, due to the application of DCD. Results indicate that due to the decrease in the operational run time by means of the application of DCD, less osmosis took place, resulting in a higher concentration factor, with respect to an FCD.

Fig. 7A presents the NH_4^+ current efficiency over the NH_4^+ concentration gradient for the DCD SBE. If Na^+ from the electrolyte ended up in the diluate and was transported to the concentrate, it would account for a 24% loss in the NH_4^+ current efficiency. However, the NH_4^+ current efficiency for the first batch was 96% at an NH_4^+ concentration gradient of 2.4 g L^{-1}. This high NH_4^+ current efficiency supports our claim that the NH_4^+ current efficiency was not affected by the transport of other ions than NH_4^+, such as H^+ and Na^+. Throughout the SBE, the NH_4^+ current efficiency decreased to 83% in the tenth batch at an NH_4^+ concentration gradient of 9.8 g L^{-1}. Similar to the FCD SBE, more back-diffusion took place due to the increase in NH_4^+ concentration gradient and the increase in operational run time. However, the effect of back-diffusion on the NH_4^+ current efficiency only caused a decrease in NH_4^+ current efficiency of 13% during the DCD SBE, compared to a decrease in NH_4^+ current efficiency of 28% during the FCD SBE. Since the NH_4^+ concentration gradient was even higher for the DCD SBE than for the FCD SBE, the higher current efficiencies and the lower decrease in NH_4^+ current efficiency are assigned to the decreased operational run times during the DCD SBE. Apparently, decreasing the operational run time by the application of DCD, results in less back-diffusion compared to an FCD, leading to a higher NH_4^+ current efficiency.

The increase in operational run time and NH_4^+ concentration gradient did not affect the energy consumption for the application of DCD (5.4 ± 0.4 MJ·kg-N^{-1}), in contrast to an FCD. The increase in energy consumption due to back-diffusion was countered by the decrease of the electrical resistance, because the EC of the concentrate increased.

4.4. Perspectives and outlook

The application of DCD led to a decrease in operational run time, compared to an FCD and, therefore, decreased the effect of osmosis and back-diffusion. As a result, the NH_4^+ concentration factor increased and the energy consumption was lower, compared to the application of an FCD.

If the water permeability of the ion exchange membranes could

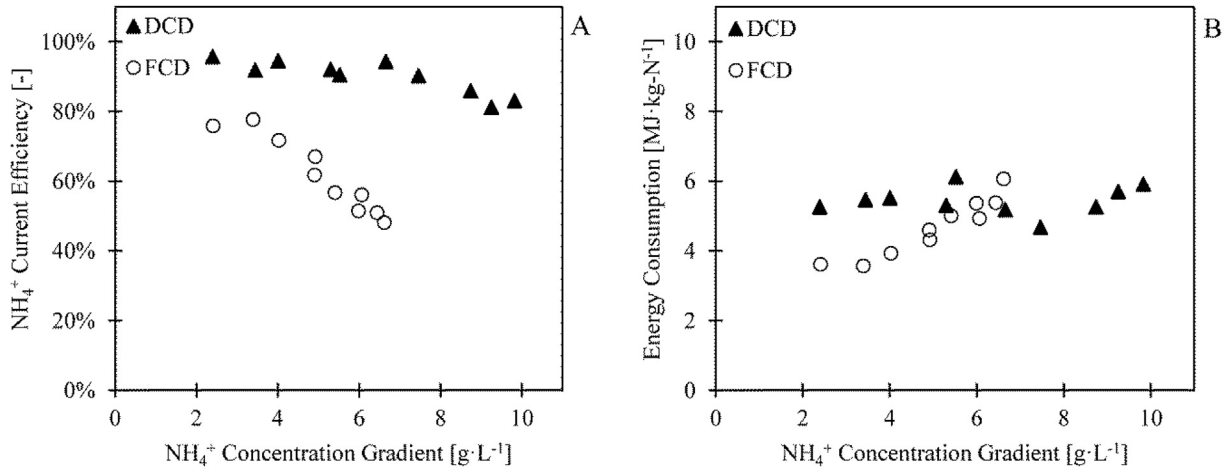

Fig. 7. The NH_4^+ current efficiency (Fig. 7A) and the energy consumption (Fig. 7B) over the NH_4^+ concentration gradient during the SBEs. The NH_4^+ current efficiency decreased during both SBEs, but the NH_4^+ current efficiency during the DCD SBE was always higher than during the FCD SBE. The energy consumption during the FCD SBE increased because the driving force for back-diffusion and the operational run time increased, while on the other, the energy consumption during the DCD SBE remained stable at 5.4 MJ·kg-N^{-1}.

be decreased, the effect of osmotic water transport can be further decreased, while an increase in electrical resistance of the ion exchange membrane should be avoided. The electrical resistance of the membrane stack can, in fact, be reduced when spacers with a low thickness or with a high void fraction are used. Besides, NH_4^+ accumulation in the electrode rinse limited the concentration factors, for both the application of FCD and DCD. By replacing the Na^+ in the initial electrode rinse with NH_4^+, accumulation of NH_4^+ in the electrode rinse can be avoided, resulting in a further increase in the concentration factor. In addition, the use of anion exchange end-membranes might also prevent the accumulation of NH_4^+ in the electrode rinse.

Based on the current results, we expect that ED can be used to remove and concentrate NH_4^+ from side streams such as reject water, at an energy consumption competitive to anammox. Since there is no (bio-)chemical conversion, recovery of NH_4^+ for e.g. fertiliser production or even energy production will be possible. Calculations show that less electrical energy was used to remove and concentrate NH_4^+ (5.4 MJ·kg-N^{-1}) than an SOFC may produce using NH_3 as fuel (13 MJ·kg-N^{-1}), assuming an electric conversion efficiency of 60%. The combination of ED, stripping and a solid oxide fuel cell could therefore potentially lead to energy-positive NH_4^+ removal from side streams.

5. Conclusions

Concentrating NH_4^+ by ED resulted in an NH_4^+ concentration gradient between the diluate and the concentrate stream. The increasing gradient subsequently resulted in increased mass transfer by osmosis and back-diffusion. The increased back-diffusion of NH_4^+ decreased the NH_4^+ current efficiency from 76% to 48% when applying an FCD and the energy consumption for the removal of 90% NH_4^+ increased from 3.6 MJ·kg-N^{-1} to 6.1 MJ·kg-N^{-1}.

When a DCD was applied, the operational run time to remove 90% NH_4^+ decreased by 75%, which can be translated to a reduction in required membrane area. The application of DCD resulted in a decrease in osmotic water transport, compared to an FCD, leading to an increased concentration factor of 6.7. When applying a DCD, the NH_4^+ current efficiency only slightly dropped over the NH_4^+ concentration gradient, i.e. from 96% to 83% and eventually 90% NH_4^+ was removed at the expense of a stable energy consumption of 5.4 MJ·kg-N^{-1}.

The results clearly show that the application of DCD allows for a lower operational run time, a higher concentration factor and a lower energy consumption to concentrate NH_4^+ by ED, compared to an FCD.

Author contributions

The manuscript was written through the contributions of all authors. N. van Linden designed and performed the experiments, analysed the results and wrote the manuscript. H. Spanjers and J.B. van Lier supervised the research and provided constructive feedback on the manuscript.

Declaration of competing interest

The authors declare that they have no known competing financial interests or personal relationships that could have appeared to influence the work reported in this paper.

Acknowledgements

This study is part of the N2kWh – From Pollutant to Power research (14712), funded by Stichting voor de Technische Wetenschappen (STW) and Instituut voor Innovatie door Wetenschap en Technologie (IWT). We thank the respective funding agencies. In addition, we thank D. Struijk for providing the Python script and R. Deckers, C. Hordijk and G. Bandinu for their assistance in the execution of the experiments.

Appendix A. Supplementary data

Supplementary data to this article can be found online at https://doi.org/10.1016/j.watres.2019.114856.

References

Brugé, F., Bernasconi, M., Parrinello, M., 1999. Ab initio simulation of rotational dynamics of solvated ammonium ion in water. J. Am. Chem. Soc. 121 (47), 10883–10888. https://doi.org/10.1021/ja990520y.

Cinti, G., Discepoli, G., Sisani, E., Desideri, U., 2016. SOFC operating with ammonia: stack test and system analysis. Int. J. Hydrogen Energy 41 (31), 13583–13590. https://doi.org/10.1016/j.ijhydene.2016.06.070.

Cowan, D.A., Brown, J.H., 1959. Effect of turbulence on limiting current in electrodialysis cells. Ind. Eng. Chem. 51 (12), 1445–1448. https://doi.org/10.1021/ie50600a026.

El-Bourawi, M.S., Khayet, M., Ma, R., Ding, Z., Li, Z., Zhang, X., 2007. Application of vacuum membrane distillation for ammonia removal. J. Membr. Sci. 301 (1–2), 200–209. https://doi.org/10.1016/j.memsci.2007.06.021.

He, Q., Tu, T., Yan, S., Yang, X., Duke, M., Zhang, Y., Zhao, S., 2018. Relating water vapor transfer to ammonia recovery from biogas slurry by vacuum membrane distillation. Separ. Purif. Technol. 191 (Suppl. C), 182–191. https://doi.org/10.1016/j.seppur.2017.09.030.

Ippersiel, D., Mondor, M., Lamarche, F., Tremblay, F., Dubreuil, J., Masse, L., 2012. Nitrogen potential recovery and concentration of ammonia from swine manure using electrodialysis coupled with air stripping. J. Environ. Manag. 95, S165–S169. https://doi.org/10.1016/j.jenvman.2011.05.026.

ISPT, 2017. Power to Ammonia: from Renewable Energy to CO2-free Ammonia as Chemical Feedstock and Fuel [Press release]. Retrieved from. http://www.ispt.eu/media/P2A-press-release-March-2017.pdf.

Kuntke, P., Sleutels, T.H.J.A., Rodríguez Arredondo, M., Georg, S., Barbosa, S.G., ter Heijne, A., Hamelers, H.V.M., Buisman, C.J.N., 2018. (Bio)electrochemical ammonia recovery: progress and perspectives. Appl. Microbiol. Biotechnol. 102 (9), 3865–3878. https://doi.org/10.1007/s00253-018-8888-6.

Lackner, S., Gilbert, E.M., Vlaeminck, S.E., Joss, A., Horn, H., van Loosdrecht, M.C.M., 2014. Full-scale partial nitritation/anammox experiences - an application survey. Water Res. 55, 292–303. https://doi.org/10.1016/j.watres.2014.02.032.

Leung, K., Nielsen, I.M.B., Kurtz, I., 2007. Ab initio molecular dynamics study of carbon dioxide and bicarbonate hydration and the nucleophilic attack of hydroxide on CO2. J. Phys. Chem. B 111 (17), 4453–4459. https://doi.org/10.1021/jp068475l.

Magri, A., Beline, F., Dabert, P., 2013. Feasibility and interest of the anammox process as treatment alternative for anaerobic digester supernatants in manure processing–an overview. J. Environ. Manag. 131, 170–184. https://doi.org/10.1016/j.jenvman.2013.09.021.

Mehta, C.M., Khunjar, W.O.F., Nguyen, V., Tait, S., Batstone, D.J., 2015. Technologies to recover nutrients from waste streams: a critical review. Crit. Rev. Environ. Sci. Technol. 45 (4), 385–427. https://doi.org/10.1080/10643389.2013.866621.

Mondor, M., Masse, L., Ippersiel, D., Lamarche, F., Massé, D.I., 2008. Use of electrodialysis and reverse osmosis for the recovery and concentration of ammonia from swine manure. Bioresour. Technol. 99 (15), 7363–7368. https://doi.org/10.1016/j.biortech.2006.12.039.

PCA, 2016. PCA Ion Exchange Membranes: Technical Data Sheet. Retrieved from. https://www.pca-gmbh.com/publi/PCAMembranes.pdf.

Pronk, W., Biebow, M., Boller, M., 2006. Electrodialysis for recovering salts from a urine solution containing micropollutants. Environ. Sci. Technol. 40 (7), 2414–2420. https://doi.org/10.1021/es051921i.

Rottiers, T., Ghyselbrecht, K., Meesschaert, B., Van der Bruggen, B., Pinoy, L., 2014. Influence of the type of anion membrane on solvent flux and back diffusion in electrodialysis of concentrated NaCl solutions. Chem. Eng. Sci. 113, 95–100. https://doi.org/10.1016/j.ces.2014.04.008.

Stambouli, A.B., Traversa, E., 2002. Solid oxide fuel cells (SOFCs): a review of an environmentally clean and efficient source of energy. Renew. Sustain. Energy Rev. 6 (5), 433–455. https://doi.org/10.1016/S1364-0321(02)00014-X.

Strathmann, H., 2004a. Chapter 2 - Electrochemical and Thermodynamic Fundamentals Ion-Exchange Membrane Separation Processes, 9 ed. Elsevier, pp. 23–88.

Strathmann, H., 2004b. Chapter 3 - Preparation and Characterization of Ion-Exchange Membranes Ion-Exchange Membrane Separation Processes, 9 ed. Elsevier, pp. 89–146.

Strathmann, H., 2004c. Chapter 4 - Operating Principle of Electrodialysis and Related Processes Ion-Exchange Membrane Separation Processes, 9 ed. Elsevier, pp. 147–225.

Strathmann, H., 2004d. Chapter 5 - Ion-Exchange Membrane Process and Equipment Design Ion-Exchange Membrane Separation Processes, 9 ed. Elsevier, pp. 227–286.

Strathmann, H., 2010. Electrodialysis, a mature technology with a multitude of new applications. Desalination 264 (3), 268–288. https://doi.org/10.1016/j.desal.2010.04.069.

Van Hulle, S.W.H., Vandeweyer, H.J.P., Meesschaert, B.D., Vanrolleghem, P.A., Dejans, P., Dumoulin, A., 2010. Engineering aspects and practical application of autotrophic nitrogen removal from nitrogen rich streams. Chem. Eng. J. 162 (1), 1–20. https://doi.org/10.1016/j.cej.2010.05.037.

Wang, X., Zhang, X., Wang, Y., Du, Y., Feng, H., Xu, T., 2015. Simultaneous recovery of ammonium and phosphorus via the integration of electrodialysis with struvite reactor. J. Membr. Sci. 490, 65–71. https://doi.org/10.1016/j.memsci.2015.04.034.

Ward, A.J., Arola, K., Thompson Brewster, E., Mehta, C.M., Batstone, D.J., 2018. Nutrient recovery from wastewater through pilot scale electrodialysis. Water Res. 135, 57–65. https://doi.org/10.1016/j.watres.2018.02.021.

Wojcik, A., Middleton, H., Damopoulos, I., Van herle, J., 2003. Ammonia as a fuel in solid oxide fuel cells. J. Power Sources 118 (1–2), 342–348. https://doi.org/10.1016/S0378-7753(03)00083-1.